Antiferromagnetic Topological Insulator with Nonsymmorphic Protection in Two Dimensions

Chengwang Niu,[1] Hao Wang,[1] Ning Mao,[1] Baibiao Huang,[1] Yuriy Mokrousov[ORCID],[2,3] and Ying Dai[1,*]

[1]*School of Physics, State Key Laboratory of Crystal Materials, Shandong University, Jinan 250100, China*
[2]*Peter Grünberg Institut and Institute for Advanced Simulation, Forschungszentrum Jülich and JARA, Jülich 52425, Germany*
[3]*Institute of Physics, Johannes Gutenberg University Mainz, Mainz 55099, Germany*

The recent demonstration of topological states in antiferromagnets (AFMs) provides an exciting platform for exploring prominent physical phenomena and applications of antiferromagnetic spintronics. A famous example is the AFM topological insulator (TI) state, which, however, was still not observed in two dimensions. Using a tight-binding model and first-principles calculations, we show that, in contrast to previously observed AFM topological insulators in three dimensions, an AFM TI can emerge in two dimensions as a result of a nonsymmorphic symmetry that combines the twofold rotation symmetry and half-lattice translation. Based on the spin Chern number, Wannier charge centers, and gapless edge states analysis, we identify intrinsic AFM XMnY (X = Sr and Ba, Y = Sn and Pb) quintuple layers as experimentally feasible examples of predicted topological states with a stable crystal structure and giant magnitude of the nontrivial band gaps, reaching as much as 186 meV for SrMnPb, thereby promoting these systems as promising candidates for innovative spintronics applications.

The interplay between symmetry and topology has been a focus of recent interest, with a variety of topological states constantly proposed and intensively explored [1–5]. The $\mathbb{Z}_2$ topological insulator (TI) state, ensured by the time-reversal symmetry $\mathcal{T}$ [6,7], has been a conceptual milestone of complex topological states, laying out appealing strategies for achieving exotic topological phenomena and realizing novel families of spintronic devices [8–10]. Manifestly, $\mathcal{T}$ symmetry breaking ($\mathcal{T}$ breaking), associated with the coexistence of topology with magnetism, plays a central role in achieving these goals via realization of, e.g., the quantum anomalous Hall effect [11,12], Majorana fermions [13], magnetic Weyl semimetals [14,15], and mixed topological semimetals [16,17].

Antiferromagnetism (AFM), on the other hand, acting as a distinct flavor of magnetic order and yielding $\mathcal{T}$ breaking, has recently drawn significant attention with respect to various spintronics applications, thereby launching the field of AFM spintronics [18–20]. The experimental observation of electrical switching of an AFM by spin-orbit torque [21], the achievement of large spin and anomalous Hall effects [22–24], and the giant magneto-optical Kerr effect [25,26] represent promising perspectives for the implementation of AFMs in spintronic devices. Remarkably, involving the interplay between AFM, symmetry, and topology, several AFM topological states with novel physical properties have been proposed [27–33]. A notable example is the AFM TI [33–38], the concept of which was worked out some years ago in seminal works by Mong *et al.* [33], and which was recently observed experimentally in three-dimensional

(3D) MnBi$_2$Te$_4$ [37,38]. For later AFM TIs, even though $\mathcal{T}$ is broken, the $T_{1/2}\mathcal{T}$ symmetry (where $T_{1/2}$ is the operator of translation by half of a lattice constant) protects the topological phase and gives rise to the $\mathbb{Z}_2$ classification of insulating AFM phases. Furthermore, as reported for MnBi$_2$Te$_4$, the axion state as well as the quantized topological magnetoelectric effect could be allowed in AFM TIs [34–36].

In two dimensions (2D), where the 2D materials have emerged as promising candidates for high-efficiency, high-density, and low power-consuming spintronic devices, an AFM topological phase exhibiting the quantum spin Hall effect is reported to coexist with the superconductivity in FeSe monolayers [39]. However, the inverted gap lies below the Fermi level for FeSe, and no realistic material candidate for 2D AFM TI has been reported yet [39,40]. This is despite the fact that it was proposed some years ago to emerge from model considerations as a result of the conserved combination of $T_{1/2}\mathcal{T}$ and space inversion $\mathcal{P}$ symmetries [41]. On the other hand, nonsymmorphic symmetry has been theoretically shown to be an alternative foundation for providing a $\mathbb{Z}_2$ classification of insulating phases of 3D AFMs [42]. In the latter case, the nonsymmporphic symmetry results in the formation of effective doublet pairs of states which replace the $T_{1/2}\mathcal{T}$-originated Kramers pairs in giving rise to TI classification. Therefore, a natural question arises as to whether the nonsymmorphic symmetry can result in the emergence of the AFM TI in two dimensions.

In this Letter, we predict that XMnY (X = Sr and Ba, Y = Sn and Pb) quintuple layers (QLs) are a family of

long-awaited intrinsic nonsymmorphic 2D AFM TIs. Remarkably, unlike previous AFM TIs, which are protected by $T_{1/2}\mathcal{T}$ symmetry, the topological phase of XMnY QLs is protected by the nonsymmorphic symmetry. We find that the nontrivial gap and Néel temperature can be as large as 186 meV and 340 K, respectively, for SrMnPb, indicating the high possibility of room-temperature observation of the nonsymmorphic AFM TI state. A four-band tight-binding model is constructed to demonstrate the feasibility of attaining this type of 2D AFM TI. Our results indicate that 2D antiferromagnets provide a very promising platform to achieve topologically complex insulating materials for AFM spintronics.

It has long been known that a TI phase can be obtained through a gap opening induced in a topological semimetal. The most famous example is graphene, where the Dirac point is protected by symmetry, but only when the spin-orbit coupling (SOC) is neglected, and a 2D TI is obtained when switching the SOC on [6]. Following this line of thought, we start with a 2D Dirac semimetal with SOC, in which the appearance of the Dirac point strongly depends on the combination of $\mathcal{T}$ and nonsymmorphic symmetry [43], and we argue that the topologically nontrivial insulators can indeed be obtained by introducing the AFM ordering to break $\mathcal{T}$. Below we show that in this way the nonsymmorphic symmetry can give rise to nontrivial band topology, as manifested in the 2D antiferromagnet. To do this, we start from a four-band tight-binding model with an intralayer out-of-plane AFM ordering [43,44]:

$$H = [\mathrm{Re}(M)\tau_x - \mathrm{Im}(M)\tau_y]\sigma_0 - 2t_{\mathrm{in}}(\cos k_x + \cos k_y)\tau_z\sigma_z$$
$$+ t_{\mathrm{SOC}}\tau_z(\sigma_y \sin k_x - \sigma_x \sin k_y) + \lambda_{\mathrm{mag}}\tau_z\sigma_z, \qquad (1)$$

which is sketched in Fig. 1(a). Here, $M = (t_1 + t_2 e^{ik_y}) \times (1 + e^{-ik_x})$. τ_α and σ_α are the Pauli matrices of the sublattices (A and B) and spin degrees of freedom. Clearly, $T_{1/2}\mathcal{T}$ symmetry is broken when the hopping energy $t_1 \neq t_2$ in the first term, and thus $t_1 = 0.7$ eV and $t_2 = 0.4$ eV are used in our model calculations. The second and third terms represent the intrinsic and Rashba SOC, respectively, and the fourth term represents the AFM ordering with an out-of-plane easy axis.

First, we show that neglecting the AFM ordering, $\lambda_{\mathrm{mag}} = 0$ eV, the above model hosts a Dirac semimetal phase as shown in Fig. 1(b), with one Dirac point at the X point. In our case, the Dirac point relies on the non-symmorphic symmetry $\{C_{2x}|\frac{1}{2}0\}$, where C_{2x} is the twofold screw symmetry and $(\frac{1}{2}0)$ is half of the lattice translation along the x axis [43]. To analyze the role of $\mathcal{T}$ breaking, we switch on the AFM term ($\lambda_{\mathrm{mag}} = -0.4$ eV). We find that the conduction and valence bands are no longer degenerate at the X point, as illustrated in Fig. 1(c). It is clear that the effect of $\mathcal{T}$ breaking is to lift the fourfold Dirac band crossing, resulting in the presence of an insulating state. As
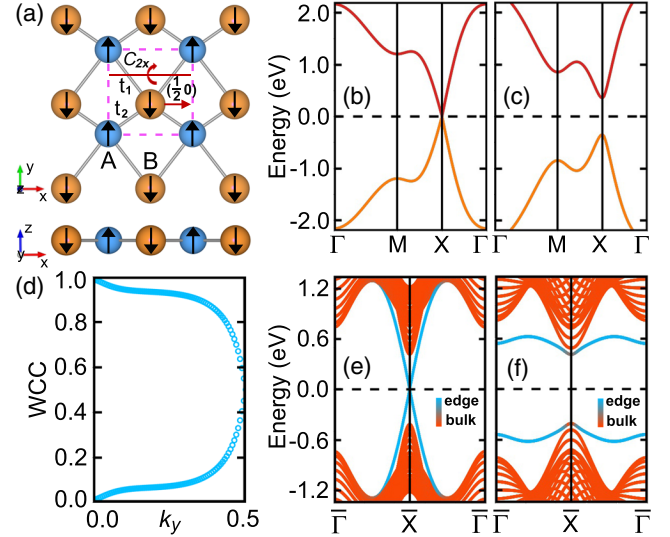

FIG. 1. (a) Sketch of the tight-binding model for a 2D antiferromagnet on a square lattice. C_{2x} represents a twofold screw symmetry and $(\frac{1}{2}0)$ denotes a half of the lattice translation along the x axis. Band structures (b) without and (c) with out-of-plane antiferromagnetism. The Dirac semimetal with the conduction and valence bands touching at X is obtained without antiferromagnetism, while a nontrivial gap opens for the case with antiferromagnetism. (d) and (e) display the Wannier charge centers (WCCs) and edge states with the nonsymmorphic symmetry $\{C_{2x}|\frac{1}{2}0\}$. (f) A gap opens up in the spectrum of a one-dimensional nanoribbon without $\{C_{2x}|\frac{1}{2}0\}$. The color transition from red to blue represents the weight of atoms located from the middle to one edge of the ribbon structures.

displayed in Figs. 1(d) and 1(e), the topologically nontrivial nature of the gap can be explicitly confirmed via calculations of the Wannier charge center (WCC) which result in $\mathbb{Z}_2 = 1$ [42], and the emergence of the exotic edge states in the nanoribbons with $\{C_{2x}|\frac{1}{2}0\}$ symmetry at the edges. Moreover, a gap opens up in the edge states when the protecting symmetry is not compatible with the termination of the one-dimensional nanoribbon, shown in Fig. 1(f), and/or is broken under distortions such as $H_c = t_c\tau_x \sin(k_x/2)\sin(k_y/2)$ [45]. Therefore, starting from a 2D Dirac semimetal, the system undergoes a topological metal-insulator transition when the AFM order is introduced, leading to the nonsymmorphic 2D AFM TI state.

Having demonstrated the possibility of a nonsymmorphic 2D AFM TI from a generic model, we aim now at the realization of 2D intrinsic antiferromagnets that exhibit the anticipated effect. The first-principles calculations with the density functional theory with the Hubbard U parameter method, which is extensively applied for the investigations of 2D magnetic materials [46–48], have been performed using the full-potential linearized augmented-plane-wave method, as implemented in FLEUR code [49] with the lattice parameters obtained using the Vienna *ab initio* simulation package [50]. The generalized gradient approximation
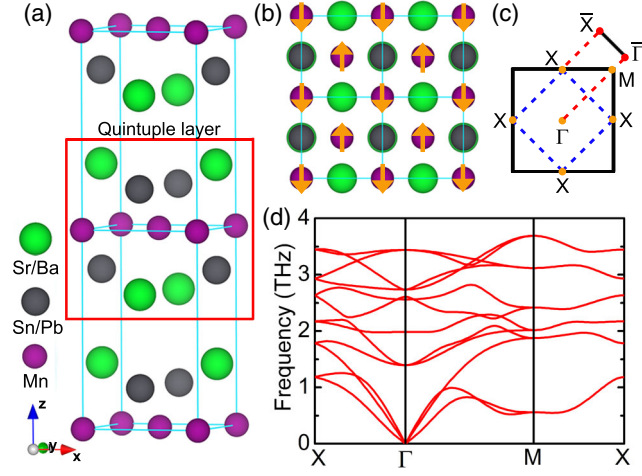
FIG. 2. (a) The side view of bulk ternary manganese compounds XMnY in space group $P4/nmm$, with a layered structure consisting of stacked QLs. (b) Top view of a QL with AFM ordering of Mn atoms. The arrows denote the atomic spin moments aligned or antialigned with the z axis. (c) 2D Brillouin zones for the unit cell (solid square) and $\sqrt{2} \times \sqrt{2}$ supercell (dashed square), and projected 1D Brillouin zone with marked high symmetry points. (d) Phonon dispersion of a SrMnPb QL, showing that the QL is dynamically stable.

TABLE I. Relaxed lattice constant a_0 (Å) of XMnY QLs, and their binding energy E_B (meV/Å^2), exchange energy E_{ex} (meV), $E_{ex} = E_{FM} - E_{AFM}$, magnetic anisotropy E_{MAE} (meV), Néel temperature T_N (K), band gaps with SOC based on PBE E_{PBE} (meV) and HSE06 E_{HSE} (meV), and spin Chern number C_S at the corresponding lattice constant.

Compounds	a_0	E_B	E_{ex}	E_{MAE}	T_N	E_{PBE}	E_{HSE}	C_S
SrMnSn	4.44	20	453	0.33	290	88	101	1
SrMnPb	4.65	39	531	1.28	340	147	186	1
BaMnSn	4.61	26	334	0.67	210	51	66	1
BaMnPb	4.68	27	401	0.48	260	94	118	1

(GGA) of Perdew, Burke, and Ernzerhof (PBE) is used for the exchange correlation potential [51]. The phonon calculations are carried out by using the density functional perturbation theory as implemented in the PHONOPY package [52]. The maximally localized Wannier functions (MLWFs) are constructed using WANNIER 90 code in conjunction with FLEUR code [53,54].

In the past, numerous investigations have been directed at manganese compounds due to diverse magnetic properties that they give rise to, among which one has to mention the observation of the giant spin-orbit torque, unusual anomalous Hall effect, and Dirac semimetal states [27,28,55–58]. Ternary manganese compounds XMnY, of which SrMnSn has already been synthesized experimentally [59], crystallize in tetragonal crystal structure with space group $P4/nmm$ and exhibit a layered structure stacked along the z axis of the square lattice, shown in Fig. 2(a), consisting of six atoms with two Mn atoms in the middle of each QL. The van der Waals interaction between the QLs provides a natural weak interlayer interaction which makes XMnY good candidates for exfoliation. We have calculated the interlayer binding energies E_B for all XMnY compounds, presenting the results in Table I. The calculated binding energies, which are further confirmed by performing density functional theory calculations with van der Waals corrections, are in the typical range for the van der Waals layered compounds and are similar to those of graphite and MoS$_2$ ($\sim$12 and $\sim$26 meV/Å^2, respectively [60,61]). The comparably small values of E_B suggest that the experimental fabrication of XMnY QLs is possible simply by exfoliation

from the layered bulk [62]. Their dynamic stability was further investigated through the phonon spectrum calculations. All phonon branches are positive in the entire Brillouin zone, as shown in Fig. 2(d) for SrMnPb, indicating that the XMnY QLs are dynamically stable and difficult to destroy once formed [45].

The calculations of magnetic properties of XMnY QLs show that the magnetic moments on each Mn are about $5\mu_B$, and therefore the Mn are in a half filled $3d^5$ configuration, leading to intrinsic antiferromagnetism. This is further verified by the calculations of the total energy difference between the ferromagnetic (FM) and AFM states of XMnY QLs listed in Table I. The large values of the exchange energy difference $E_{ex} = E_{FM} - E_{AFM}$ indicate that the observed AFM ordering is strong and robust. Taking into account the SOC, magnetic anisotropy energy E_{MAE} was also calculated. For all XMnY QLs, AFM ordering with an out-of-plane direction of staggered magnetization is shown to be the most energetically stable. Furthermore, based on a Heisenberg Hamiltonian with a nearest-neighbor AFM interaction, the Néel temperature of the studied compounds was estimated from Monte Carlo simulations to be as large as 340 K, implying the possibility of potential applications at room temperature [45].

Given the AFM ground state, taking SrMnPb QL as an example, we present in Figs. 3(a) and 3(b) the orbitally resolved band structure without and with SOC. The minority and majority spin bands are degenerate in the absence of SOC, confirming the AFM ordering without net magnetic moments [45]. Mn-d_{yz} and Mn-d_{zx} orbitals are doubly degenerate as a result of the D_{2d} symmetry of the crystal group and contribute to the valence-band maximum, while the conduction-band minimum is dominated by a single Mn-d_{z^2} orbital with a small direct band gap of 12 meV. Switching on SOC leads to the inversion of the orbital character around the Γ point, and a d-d band inversion occurs which is qualitatively different from the s-p or p-p band inversions in nonmagnetic TIs [8–10]. In electronic systems, although it is not a sufficient condition, such band inversion is an important mechanism for the formation of a nontrivial topological phase [63]. The bands remain doubly degenerate in this case, and, remarkably, the
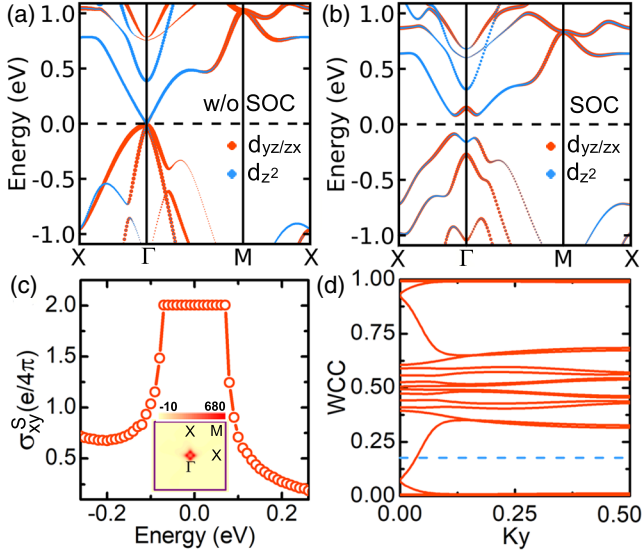
FIG. 3. Orbitally resolved band structures for SrMnPb QLs (a) without and (b) with SOC, weighted with the contribution of Mn-$d_{yz/zx}$ and Mn-d_{z^2} states. The Fermi level is indicated with a dashed line. (c) Energy dependence of the spin Hall conductivity σ_{xy}^S, showing a quantized value within the energy window of the SOC gap. (Inset) K-space distribution of spin Berry curvature within the SOC gap. (d) Evolution of WCCs for SrMnPb QLs along k_y, confirming the topological nature of the gap with $\mathbb{Z}_2 = 1$.

insulating character is preserved with a band gap of 147 meV, implying that SrMnPb is potentially a topologically nontrivial insulator. As summarized in Table I, the insulating states emerge in all of the studied XMnY QLs [45]. To further confirm our results, band structures are checked by using the more sophisticated Heyd-Scuseria-Ernzerhof hybrid functional method (HSE06) [64]. Larger band gaps are obtained for all XMnY QLs, with the band inversions remaining intact at the Γ point, as shown in Table I.

To confirm the topologically nontrivial character of the gap, the spin Hall conductivity σ_{xy}^S is calculated using the Kubo formula [65]:

$$\sigma_{xy}^S = e\hbar \int \frac{d^2k}{(2\pi)^2} \Omega^S(\mathbf{k}),$$

$$\Omega^S(\mathbf{k}) = -2\mathrm{Im}\sum_{m \neq n} \frac{\langle \psi_{m\mathbf{k}} | J_x^S | \psi_{n\mathbf{k}} \rangle \langle \psi_{n\mathbf{k}} | v_y | \psi_{m\mathbf{k}} \rangle}{(E_{n\mathbf{k}} - E_{m\mathbf{k}})^2}. \quad (2)$$

Here, v_i is the ith Cartesian component of the velocity operator, $|\psi_{n\mathbf{k}}\rangle$ is an eigenstate of the lattice-periodic Hamiltonian with energy $E_{n\mathbf{k}}$, and $J_x^s = (\hbar/4)\{\sigma^z, v_x\}$ describes a spin current flowing in the x direction, with the spin polarization perpendicular to the plane. In the respective insulating regions, σ_{xy}^S is analogous to the spin

Chern number $\mathcal{C}_S$, where $\mathcal{C}_S = (\mathcal{C}_+ - \mathcal{C}_-)/2$, with $\mathcal{C}_+$ and $\mathcal{C}_-$ being Chern numbers of the spin-up and spin-down manifolds, allowing for the alternative representation $\sigma_{xy}^S = \mathcal{C}_S e/(2\pi)$ and leading to a $\mathbb{Z}_2$ classification of the electronic structure [66]. Figure 3(c) displays the σ_{xy}^S as a function of the Fermi level in a SrMnPb QL. The quantization of σ_{xy}^S within the insulating region, which arises mainly from the spin Berry curvature $\Omega^S(\mathbf{k})$ near the Γ point, as shown in the inset of Fig. 3(c), is clearly visible, demonstrating the nontrivial band topology of SrMn$_2$Bi$_2$ QLs. The nonzero σ_{xy}^S ($\mathcal{C}_S$) is further confirmed by our WCC calculations, as plotted in Fig. 3(d) [67], where the number of crossings between the WCC and the reference horizontal line is odd.

While the previously reported AFM TIs are usually associated with $T_{1/2}\mathcal{T}$ and, in addition, it is expected that crystalline mirror symmetries can give rise to an AFM TI state [68] (although the material realization is still missing here), both of them are broken in AFM XMnY QLs, as shown in Figs. 2(a) and 2(b). Remarkably, as we show below, the nonsymmorphic $\{C_{2x}|\frac{1}{2}0\}$ symmetry is preserved in XMnY QLs, and it protects their TI state. To validate the symmetry protection of the discovered AFM TI state, different AFM configurations which either keep or break the $\{C_{2x}|\frac{1}{2}0\}$ symmetry were considered. We first consider changing the electronic structure via the magnetization direction, which has been demonstrated to have a dramatic impact on topology [16,17,28]. When we change the direction of the staggered magnetization from out of plane to in plane, the electronic bands remain doubly degenerate, and the AFM TI state in XMnY remains intact since the $\{C_{2x}|\frac{1}{2}0\}$ symmetry survives in this case. We then consider an AFM configuration with Mn atoms coupling antiferromagnetically along the x and y directions, thus breaking the $\{C_{2x}|\frac{1}{2}0\}$ symmetry. A trivial metallic state is obtained in this case, confirming clearly that the AFM TI is protected by the $\{C_{2x}|\frac{1}{2}0\}$ symmetry [45]. It is interesting to note that, while the strain is an effective approach to modulate the electronic and topological properties, the hydrostatic strain can go up to as much as $\pm 6\%$ before it destroys the AFM TI state [45]. Such robust against lattice deformation AFM topology makes XMnY an attractive, stable candidate for experimental observation and device applications.

As a further confirmation of the topologically nontrivial phase, the edge states are calculated using the MLWFs of $\sqrt{2} \times \sqrt{2}$ supercells of XMnY QLs, in which the non-symmorphic $\{C_{2x}|\frac{1}{2}0\}$ symmetry survives [67]. Figure 4 displays the results for the semi-infinite XMnY QLs terminated by Sr/Ba and Sn/Pb atoms. One can clearly see that a pair of gapless edge states crosses at the $\bar{\Gamma}$ point for all of the XMnY QLs. This is in direct agreement with the calculated values of spin Chern number $\mathcal{C}_S = 1$. Their spin polarization is then checked by computing the matrix elements of the Pauli matrices σ_z in the basis of the MLWFs. Similar to the helical edge states in 2D TIs, the edge states of 2D AFM TIs
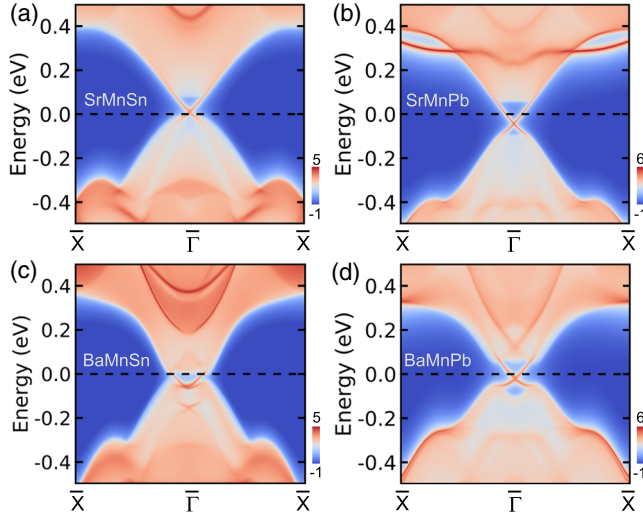
FIG. 4.   Calculated LDOS of edge states terminated by Sr/Ba and Sn/Pb atoms for (a) SrMnSn, (b) SrMnPb, (c) BaMnSn, and (d) BaMnPb QLs with SOC. The color range from blue to red represents the higher LDOS. Topological edge states can be clearly seen for all considered QLs around the $\bar{\Gamma}$ point.

that we found are spin polarized, with the spin polarization direction locked with their momentum.

In summary, we theoretically demonstrated that XMnY QLs are a family of promising material candidates for nonsymmorphic 2D AFM TIs. On the one hand, XMnY QLs are stable 2D AFM materials which are experimentally feasible to achieve from layered van der Waals compounds. On the other hand, XMnY QLs hold topologically insulating states with a giant energy gap. Their nontrivial topology can be characterized by spin Chern number $\mathcal{C}_S = 1$ Wannier charge centers, as well as gapless helical edge states, and it is robust against perturbations preserving the $\{C_{2x}|\frac{1}{2}0\}$ symmetry. The presented results not only advance our general understanding of magnetic topological states but also put forward potential applications in topological AFM spintronics.

*daiy60@sdu.edu.cn

[1] B. Bradlyn, L. Elcoro, J. Cano, M. G. Vergniory, Z. Wang, C. Felser, M. I. Aroyo, and B. A. Bernevig, Nature (London) **547**, 298 (2017).

[2] H. C. Po, A. Vishwanath, and H. Watanabe, Nat. Commun. **8**, 50 (2017).

[3] Z. Song, T. Zhang, Z. Fang, and C. Fang, Nat. Commun. **9**, 3530 (2018).

[4] H. Watanabe, H. C. Po, and A. Vishwanath, Sci. Adv. **4**, eaat8685 (2018).

[5] F. Tang, H. C. Po, A. Vishwanath, and X. Wan, Sci. Adv. **5**, eaau8725 (2019).

[6] C. L. Kane and E. J. Mele, Phys. Rev. Lett. **95**, 226801 (2005).

[7] B. A. Bernevig, T. L. Hughes, and S.-C. Zhang, Science **314**, 1757 (2006).

[8] M. Z. Hasan and C. L. Kane, Rev. Mod. Phys. **82**, 3045 (2010).

[9] X.-L. Qi and S.-C. Zhang, Rev. Mod. Phys. **83**, 1057 (2011).

[10] A. Bansil, H. Lin, and T. Das, Rev. Mod. Phys. **88**, 021004 (2016).

[11] R. Yu, W. Zhang, H.-J. Zhang, S.-C. Zhang, X. Dai, and Z. Fang, Science **329**, 61 (2010).

[12] C.-Z. Chang *et al.*, Science **340**, 167 (2013).

[13] L. Fu and C. L. Kane, Phys. Rev. Lett. **100**, 096407 (2008).

[14] G. Xu, H. Weng, Z. Wang, X. Dai, and Z. Fang, Phys. Rev. Lett. **107**, 186806 (2011).

[15] Z. Wang, M. G. Vergniory, S. Kushwaha, M. Hirschberger, E. V. Chulkov, A. Ernst, N. P. Ong, R. J. Cava, and B. A. Bernevig, Phys. Rev. Lett. **117**, 236401 (2016).

[16] J.-P. Hanke, F. Freimuth, C. Niu, S. Blügel, and Y. Mokrousov, Nat. Commun. **8**, 1479 (2017).

[17] C. Niu, J.-P. Hanke, P. M. Buhl, H. Zhang, L. Plucinski, D. Wortmann, S. Blügel, G. Bihlmayer, and Y. Mokrousov, Nat. Commun. **10**, 3179 (2019).

[18] T. Jungwirth, X. Marti, P. Wadley, and J. Wunderlich, Nat. Nanotechnol. **11**, 231 (2016).

[19] L. Šmejkal, Y. Mokrousov, B. Yan, and A. H. MacDonald, Nat. Phys. **14**, 242 (2018).

[20] V. Baltz, A. Manchon, M. Tsoi, T. Moriyama, T. Ono, and Y. Tserkovnyak, Rev. Mod. Phys. **90**, 015005 (2018).

[21] P. Wadley *et al.*, Science **351**, 587 (2016).

[22] W. Zhang, M. B. Jungfleisch, W. Jiang, J. E. Pearson, A. Hoffmann, F. Freimuth, and Y. Mokrousov, Phys. Rev. Lett. **113**, 196602 (2014).

[23] A. K. Nayak, J. E. Fischer, Y. Sun, B. Yan, J. Karel, A. C. Komarek, C. Shekhar, N. Kumar, W. Schnelle, J. Kübler, C. Felser, and S. S. P. Parkin, Sci. Adv. **2**, e1501870 (2016).

[24] M. Ikhlas, T. Tomita, T. Koretsune, M. T. Suzuki, D. Nishio-Hamane, R. Arita, Y. Otani, and S. Nakatsuji, Nat. Phys. **13**, 1085 (2017).

[25] W. Feng, G.-Y. Guo, J. Zhou, Y. Yao, and Q. Niu, Phys. Rev. B **92**, 144426 (2015).

[26] T. Higo, H. Man, D. B. Gopman, L. Wu, T. Koretsune, O. M. J. van 't Erve, Y. P. Kabanov, D. Rees, Y. Li, M. T. Suzuki, S. Patankar, M. Ikhlas, C. L. Chien, R. Arita, R. D. Shull, J. Orenstein, and S. Nakatsuji, Nat. Photonics **12**, 73 (2018).

[27] P. Tang, Q. Zhou, G. Xu, and S.-C. Zhang, Nat. Phys. **12**, 1100 (2016).

[28] L. Šmejkal, J. Železný, J. Sinova, and T. Jungwirth, Phys. Rev. Lett. **118**, 106402 (2017).

[29] S. M. Young and B. J. Wieder, Phys. Rev. Lett. **118**, 186401 (2017).

[30] K. Jiang, S. Zhou, X. Dai, and Z. Wang, Phys. Rev. Lett. **120**, 157205 (2018).

[31] D.-F. Shao, G. Gurung, S.-H. Zhang, and E. Y. Tsymbal, Phys. Rev. Lett. **122**, 077203 (2019).

[32] J. Liu, S. Meng, and J.-T. Sun, Nano Lett. **19**, 3321 (2019).

[33] R. S. K. Mong, A. M. Essin, and J. E. Moore, Phys. Rev. B **81**, 245209 (2010).

[34] M. M. Otrokov, I. P. Rusinov, M. Blanco-Rey, M. Hoffmann, A. Y. Vyazovskaya, S. V. Eremeev, A. Ernst, P. M. Echenique, A. Arnau, and E. V. Chulkov, Phys. Rev. Lett. **122**, 107202 (2019).

[35] D. Zhang, M. Shi, T. Zhu, D. Xing, H. Zhang, and J. Wang, Phys. Rev. Lett. **122**, 206401 (2019).

[36] J. Li, Y. Li, S. Du, Z. Wang, B. L. Gu, S. C. Zhang, K. He, W. Duan, and Y. Xu, Sci. Adv. **5**, eaaw5685 (2019).

[37] Y. Gong *et al.*, Chin. Phys. Lett. **36**, 076801 (2019).

[38] M. M. Otrokov *et al.*, Nature (London) **576**, 416 (2019).

[39] Z. F. Wang, H. Zhang, D. Liu, C. Liu, C. Tang, C. Song, Y. Zhong, J. Peng, F. Li, C. Nie, L. Wang, X. J. Zhou, X. Ma, Q. K. Xue, and F. Liu, Nat. Mater. **15**, 968 (2016).

[40] C. Niu, J.-P. Hanke, P. M. Buhl, G. Bihlmayer, D. Wortmann, S. Blügel, and Y. Mokrousov, arXiv:1705.07035.

[41] C. Fang, M. J. Gilbert, and B. A. Bernevig, Phys. Rev. B **88**, 085406 (2013).

[42] C.-X. Liu, R.-X. Zhang, and B. K. VanLeeuwen, Phys. Rev. B **90**, 085304 (2014).

[43] S. M. Young and C. L. Kane, Phys. Rev. Lett. **115**, 126803 (2015).

[44] C.-C. Liu, H. Jiang, and Y. Yao, Phys. Rev. B **84**, 195430 (2011).

[45] See Supplemental Material at http://link.aps.org/supplemental/10.1103/PhysRevLett.124.066401 for phonon dispersions, density of states, and band structures of additional tight-binding and first-principles results.

[46] Y. Ma, Y. Dai, M. Guo, C. Niu, Y. Zhu, and B. Huang, ACS Nano **6**, 1695 (2012).

[47] N. Sivadas, S. Okamoto, X. Xu, C. J. Fennie, and D. Xiao, Nano Lett. **18**, 7658 (2018).

[48] P. Jiang, C. Wang, D. Chen, Z. Zhong, Z. Yuan, Z.-Y. Lu, and W. Ji, Phys. Rev. B **99**, 144401 (2019).

[49] See http://www.flapw.de.

[50] G. Kresse and J. Furthmüller, Phys. Rev. B **54**, 11169 (1996).

[51] J. P. Perdew, K. Burke, and M. Ernzerhof, Phys. Rev. Lett. **77**, 3865 (1996).

[52] A. Togo and I. Tanaka, Scr. Mater. **108**, 1 (2015).

[53] A. A. Mostofi, J. R. Yates, Y.-S. Lee, I. Souza, D. Vanderbilt, and N. Marzari, Comput. Phys. Commun. **178**, 685 (2008).

[54] F. Freimuth, Y. Mokrousov, D. Wortmann, S. Heinze, and S. Blügel, Phys. Rev. B **78**, 035120 (2008).

[55] H. Chen, Q. Niu, and A. H. MacDonald, Phys. Rev. Lett. **112**, 017205 (2014).

[56] S. Nakatsuji, N. Kiyohara, and T. Higo, Nature (London) **527**, 212 (2015).

[57] A. K. Nayak, J. E. Fischer, Y. Sun, B. Yan, J. Karel, A. C. Komarek, C. Shekhar, N. Kumar, W. Schnelle, J. Kübler, C. Felser, and S. S. P. Parkin, Sci. Adv. **2**, e1501870 (2016).

[58] W. Zhang, W. Han, S.-H. Yang, Y. Sun, Y. Zhang, B. Yan, and S. S. P. Parkin, Sci. Adv. **2**, e1600759 (2016).

[59] A. Dascoulidou, P. Müller, and W. Bronger, Z. Anorg. Allg. Chem. **624**, 124 (1998).

[60] T. Björkman, A. Gulans, A. V. Krasheninnikov, and R. M. Nieminen, Phys. Rev. Lett. **108**, 235502 (2012).

[61] N. Mounet, M. Gibertini, P. Schwaller, D. Campi, A. Merkys, A. Marrazzo, T. Sohier, I. E. Castelli, A. Cepellotti, G. Pizzi, and N. Marzari, Nat. Nanotechnol. **13**, 246 (2018).

[62] K. S. Novoselov, A. K. Geim, S. V. Morozov, D. Jiang, Y. Zhang, S. V. Dubonos, I. V. Grigorieva, and A. A. Firsov, Science **306**, 666 (2004).

[63] J. Li, I. Martin, M. Büttiker, and A. F. Morpurgo, Phys. Scr. **T146**, 014021 (2012).

[64] A. V. Krukau, O. A. Vydrov, A. F. Izmaylov, and G. E. Scuseria, J. Chem. Phys. **125**, 224106 (2006).

[65] J. Sinova, S. O. Valenzuela, J. Wunderlich, C. H. Back, and T. Jungwirth, Rev. Mod. Phys. **87**, 1213 (2015).

[66] Y. Yang, Z. Xu, L. Sheng, B. Wang, D. Y. Xing, and D. N. Sheng, Phys. Rev. Lett. **107**, 066602 (2011).

[67] Q. S. Wu, S. N. Zhang, H. F. Song, M. Troyer, and A. A. Soluyanov, Comput. Phys. Commun. **224**, 405 (2018).

[68] T. H. Hsieh, H. Lin, J. Liu, W. Duan, A. Bansil, and L. Fu, Nat. Commun. **3**, 982 (2012).